ADVANCES IN ATMOSPHERIC SCIENCES, VOL. 38, FEBRUARY 2021, 237–252

• **Original Paper** •

Improvement of Soil Moisture Simulation in Eurasia by the Beijing Climate Center Climate System Model from CMIP5 to CMIP6

Yinghan SANG[1,3], Hong-Li REN[*2,3], Xueli SHI[3], Xiaofeng XU[4,1], and Haishan CHEN[1]

[1]*School of Atmospheric Sciences*, *Nanjing University of Information Science & Technology*, *Nanjing* 210044, *China*

[2]*State Key Laboratory of Severe Weather*, *Chinese Academy of Meteorological Sciences*, *Beijing* 100081, *China*

[3]*Laboratory for Climate Studies & CMA–NJU Joint Laboratory for Climate Prediction Studies*, *National Climate Center*, *China Meteorological Administration*, *Beijing* 100081, *China*

[4]*China Meteorological Administration*, *Beijing* 100081, *China*

(Received 31 May 2020; revised 24 August 2020; accepted 29 September 2020)

ABSTRACT

This study provides a comprehensive evaluation of historical surface soil moisture simulation (1979–2012) over Eurasia at annual and seasonal time scales between two medium-resolution versions of the Beijing Climate Center Climate System Model (BCC-CSM)—one that is currently participating in phase 6 of the Coupled Model Intercomparison Project (CMIP6), i.e., BCC-CSM2-MR, and the other, BCC-CSM1.1m, which participated in CMIP5. We show that BCC-CSM2-MR is more skillful in reproducing the climate mean states and standard deviations of soil moisture, with pattern correlations increased and biases reduced significantly. BCC-CSM2-MR performs better in capturing the first two primary patterns of soil moisture anomalies, where the period of the corresponding time series is closer to that of reference data. Comparisons show that BCC-CSM2-MR performs at a high level among multiple models of CMIP6 in terms of centered pattern correlation and "amplitude of variation" (relative standard deviation). In general, the centered pattern correlation of BCC-CSM2-MR, ranging from 0.61 to 0.87, is higher than the multi-model mean of CMIP6, and the relative standard deviation is 0.75, which surmounts the overestimations in most of the CMIP6 models. Due to the vital role played by precipitation in land–atmosphere interaction, possible causes of the improvement of soil moisture simulation are further related to precipitation in BCC-CSM2-MR. The results indicate that a better description of the relationship between soil moisture and precipitation and a better reproduction of the climate mean precipitation by the model may result in the improved performance of soil moisture simulation.

Key words: BCC-CSM, soil moisture, CMIP6, historical simulation, Eurasia

Citation: Sang, Y. H., H.-L. Ren, X. L. Shi, X. F. Xu, and H. S. Chen, 2021: Improvement of soil moisture simulation in Eurasia by the Beijing Climate Center Climate System Model from CMIP5 to CMIP6. *Adv. Atmos. Sci.*, **38**(2), 237–252, https://doi.org/10.1007/s00376-020-0167-7.

Article Highlights:

- The new version (BCC-CSM2-MR) of the Beijing Climate Center Climate System Model for the CMIP6 historical experiment is more skillful in simulating the spatiotemporal variations of surface soil moisture, with fewer biases, compared to its previous version (BCC-CSM1.1m) in CMIP5 and most models of CMIP6.
- The improvement in surface soil moisture simulation by BCC-CSM2-MR is possibly attributable to the better performance of this model in representing the proper relationship between soil moisture and precipitation and reproducing the variation of precipitation with fewer deviations.

1. Introduction

Soil moisture (SM) plays a vital role in affecting climatic variability through influencing many physical processes in land–atmosphere interactions. By regulating surface water, evapotranspiration, and latent heat, as well as ground fluxes, SM variations feed back to the near-surface climate, extending to the boundary layer, impact vertical stability, and further affect precipitation (Seneviratne et al., 2010; Berg and Sheffield, 2018; Ruosteenoja et al., 2018). One salient character of SM is its long memory (Koster and Suarez, 2001; Shinoda, 2001; Ruosteenoja et al., 2018), which can last 30–90 days for some climatic elements (Dirmeyer et al.,

* Corresponding author: Hong-Li REN
Email: renhl@cma.gov.cn

2009). The climatic response to the variation in SM changes with regions and seasons (Yeh et al., 1984; Koster et al., 2003; Koster et al., 2004). Especially in the Eurasian continent with its complex and diverse climate, SM not only affects ground fluxes and climate in the monsoon zone, but also impacts the evaporation and water vapor transport and further the precipitation and temperature inland (Ma et al., 2000; Zuo and Zhang, 2007; Dai and Zuo, 2010; Zhang et al., 2016a).

Owing to the deficiency of reliable long-term and large-spatial-scale in-situ observational datasets, alternative data sources have been made available for researching SM variation. Represented by the Global Land Data Assimilation System (GLDAS), several assimilated SM data products have been developed. Research has found that data assimilation can significantly improve the accuracy of middle and deep SM estimates and the assimilated data products are reliable for describing the SM annual cycle and short-term variability (Renzullo et al., 2014). Simulations from offline land surface models and coupled general circulation models (GCMs) are another tool for investigating the continuity of SM spatially and temporally (Srinivasan et al., 2000; Koster et al., 2009). With the gradual improvements of model systems in the past several decades, their ability to reproduce SM has led to great progress, but there are still deficiencies. Guo and Dirmeyer (2006) pointed out that, although models can reproduce SM anomalies to a certain extent, they do not simulate absolute soil water content accurately. Xia et al. (2015) also showed that model simulations may overestimate the SM in the Northern Hemisphere. Cheng et al. (2015) analyzed the simulations of 20 CMIP5 (phase 5 of the Coupled Model Intercomparison Project) GCMs and revealed that there has been an obvious decreasing trend in annual-mean near-surface SM over eastern Asia. Research also demonstrated that the majority of CMIP5 GCMs likewise simulate soil drying in the Northern Hemisphere, for nearly the whole continent of North America in summer and everywhere apart from the Arctic regions in spring (Dirmeyer et al., 2013). Thus, although there is a certain biases, simulations based on climate models are efficient tools to investigate the variations and effects of SM in the climate system.

However, because so many models have been developed with different descriptions of land surface and SM-related schemes, under the same simulation framework, say the CMIP experiments, comparisons of multi-model simulations will provide an overall assessment of the model performance, but are inconvenient for investigating the reasons. On the contrary, comparisons of different model versions of a specified model system in the different phases of CMIP will provide a good opportunity to understand the SM simulation performance.

The Beijing Climate Center Climate System Model (BCC-CSM) is one of the fully coupled climate system models that has participated in both the CMIP5 and CMIP6 experiments. Most of the CMIP6 simulations have now been finished, with datasets available via the ESGF website (Xin et al., 2019). Wu et al. (2019) summarized the general model improvements and performances of different components of models from CMIP5 to CMIP6. However, the SM has not yet been systematically evaluated. Therefore, in this paper, we assess the SM simulated by BCC-CSM through comparisons with assimilated data and observations as well as results of the different BCC model versions. Two medium resolutions are selected for comparison here, i.e., BCC-CSM2-MR for CMIP6 and BCC-CSM1.1m for CMIP5, in the historical experiments. Then, a horizontal comparison is made between BCC-CSM2-MR and 13 CMIP6 models. Finally, the coupling between precipitation and SM in model simulations is also discussed.

2. Data and methods

2.1. *Data*

2.1.1. *BCC-CSM historical simulations in CMIP5 and CMIP6*

Recently, BCC-CSM has been upgraded to its second generation (Wu et al., 2020). The medium-resolution version (BCC-CSM2-MR) has carried out most of the CMIP6 DECK and MIP experiments (Eyring et al., 2016; Xin et al., 2019). Its previous generation (BCC-CSM1.1m; Wu et al., 2013, 2014) participated in CMIP5 (Taylor et al., 2012; Xin et al., 2012). Among the experiments endorsed by CMIP5 and CMIP6, historical simulation is one of the entry cards for models to participate in the project. The historical period is defined as beginning in 1850 and extends to near to the present day (2012 for CMIP5 and 2014 for CMIP6). The CMIP historical simulation provides a good opportunity to assess model ability in simulating climatic variability and trends. In this study, monthly surface (0–10 cm) SM data from the historical simulation of BCC-CSM2-MR are evaluated by comparing with 13 other CMIP6 models (Table 1) and BCC-CSM1.1m in CMIP5. The monthly precipitation data of the BCC-CSMs are also used, to analyze the coupling between SM and precipitation.

2.1.2. *Reference data*

Representative of assimilated SM data products, GLDAS, which comprises ingested satellite- and ground-based observational data products and uses advanced land surface modeling and data assimilation techniques (Rodell et al., 2004), is widely used in studies of land–atmosphere interaction (Cheng et al., 2013; Zhang et al., 2016b). Therefore, we select the monthly data of near-surface (0–10 cm) SM from GLDAS v2.0 and v2.1 as the reference data in this study. In addition, we also use a station-based observational SM dataset in China produced by Wang and Shi (2019), to make the best use of the observations available at present. The SM measurements at a total of 1471 stations for the period January 1992 to September 2013 are from the

Table 1. Details of the 14 CMIP6 models used in this study.

Model name	Model center (or group)	Spatial resolution (lat × lon)
BCC-CSM2-MR	Beijing Climate Center, China Meteorological Administration	160 × 320
CanESM5	Canadian Centre for Climate Modelling and Analysis	64 × 128
CESM2	Community Earth System Model Contributors	192 × 288
CESM2-WACCM	Community Earth System Model Contributors	192 × 288
E3SM-1-0	U.S. Department of Energy's Office of Biological and Environmental Research	180 × 360
EC-Earth3-Veg	EC-Earth consortium (27 institutions in Europe)	256 × 512
FGOALS-f3-L	LASG, Institute of Atmospheric Physics, Chinese Academy of Sciences	192 × 288
FIO-ESM-2-0	First Institute of Oceanography, Ministry of Natural Resources of China	192 × 288
GFDL-CM4	NOAA Geophysical Fluid Dynamics Laboratory	180 × 288
IPSL-CM6A-LR	Institut Pierre-Simon Laplace	143 × 144
MIROC6	Atmosphere and Ocean Research Institute (The University of Tokyo)	128 × 256
MRI-ESM2-0	Meteorological Research Institute	160 × 320
NorESM2-LM	Norwegian Climate Centre	96 × 144
SAM0-UNICON	The National Renewable Energy Laboratory	192 × 288

National Meteorological Information Center of the China Meteorological Administration. Among these, 732 stations with good spatial and temporal continuity from January 1992 to December 2012 are ultimately selected following quality control processes. We use the data of the first layer (0–10 cm) and transform the units into kg m^{-2} for comparison. In the analysis of the coupling between SM and precipitation, we use the monthly data of precipitation from the CPC (Climate Prediction Center of NOAA) Merged Analysis of Precipitation (CMAP; Huffman et al., 1997).

2.2. *Research region and diagnostic method*

The study region in this paper is Eurasia (10°–80°N, 30°–160°E) and the study period ranges from 1979 to 2012, in which we use the annual mean and the four seasons defined as December–January–February (DJF) for winter, March–April–May (MAM) for spring, June–July–August (JJA) for summer, and September–October–November (SON) for autumn. For convenience of comparison, both the simulation data and reference data are regrided to a uniform resolution of 1° × 1° using bilinear interpolation. Although the dataset of the 732 stations is quality controlled, there are still plenty of missing values in the spatial and temporal range. Therefore, it is inaccurate and inconvenient to interpolate the station dataset to the grid. Accordingly, when using the station dataset from 1992 to 2012 as the reference to make comparisons, we interpolate the simulation data in China to the positions of the 732 stations. Pearson correlation (r), root-mean-square error (RMSE), standard deviation and linear regression, the most commonly used metrics (Legates and McCabe, 1999), are used to quantify the agreement between reference data and model simulations. Besides, empirical orthogonal function (EOF) analysis and spectral analysis are performed to identify the major modes of the surface SM anomalies in Eurasia and its periodic characteristics.

3. Results

3.1. *Comparison between BCC-CSM2-MR and BCC-CSM1.1m*

3.1.1. *Spatial distribution in Eurasia*

The climatological mean surface SM in terms of annual mean and the four seasons of GLDAS and BCC-CSM simulations are firstly presented (Fig. 1). Basically, except the less pronounced gradient in model simulations, both BCC-CSM2-MR and BCC-CSM1.1m are able to capture the spatial patterns of the SM of GLDAS, but BCC-CSM2-MR is closer to GLDAS in terms of the higher pattern correlation. GLDAS shows a triple pattern in the annual mean, whereby the surface soil with higher soil water content is typically located in central and western Siberia and South China, while that with lower soil water content is mainly distributed in central Asia and the Arabian Peninsula (Fig. 1a). From northwest to southeast, the SM in Eurasia exhibits a wet–dry–wet distribution, which is consistent with previous research (Nijssen et al., 2001; Guo et al., 2003; Erdenebat and Sato, 2018). This pattern is also evident in the BCC-CSM2-MR and BCC-CSM1.1m model simulations (Figs. 1b and 1c). The pattern correlation coefficient between BCC-CSM2-MR and GLDAS is 0.97 (at the 0.01 significance level), which is higher than that between BCC-CSM1.1m and GLDAS (r = 0.93). In different seasons, the pattern correlation coefficients of BCC-CSM2-MR and GLDAS range from 0.96 to 0.97, which are higher than those of BCC-CSM1.1m (between 0.92 and 0.94). The average pattern correlation coefficient between BCC-CSM2-MR and GLDAS is 0.97, which is a rise of 4.3% over the previous version. Therefore, BCC-CSM2-MR is more capable than BCC-CSM1.1m in its reproduction of the distribution of the climate mean surface SM.

The difference in patterns of the climate mean SM

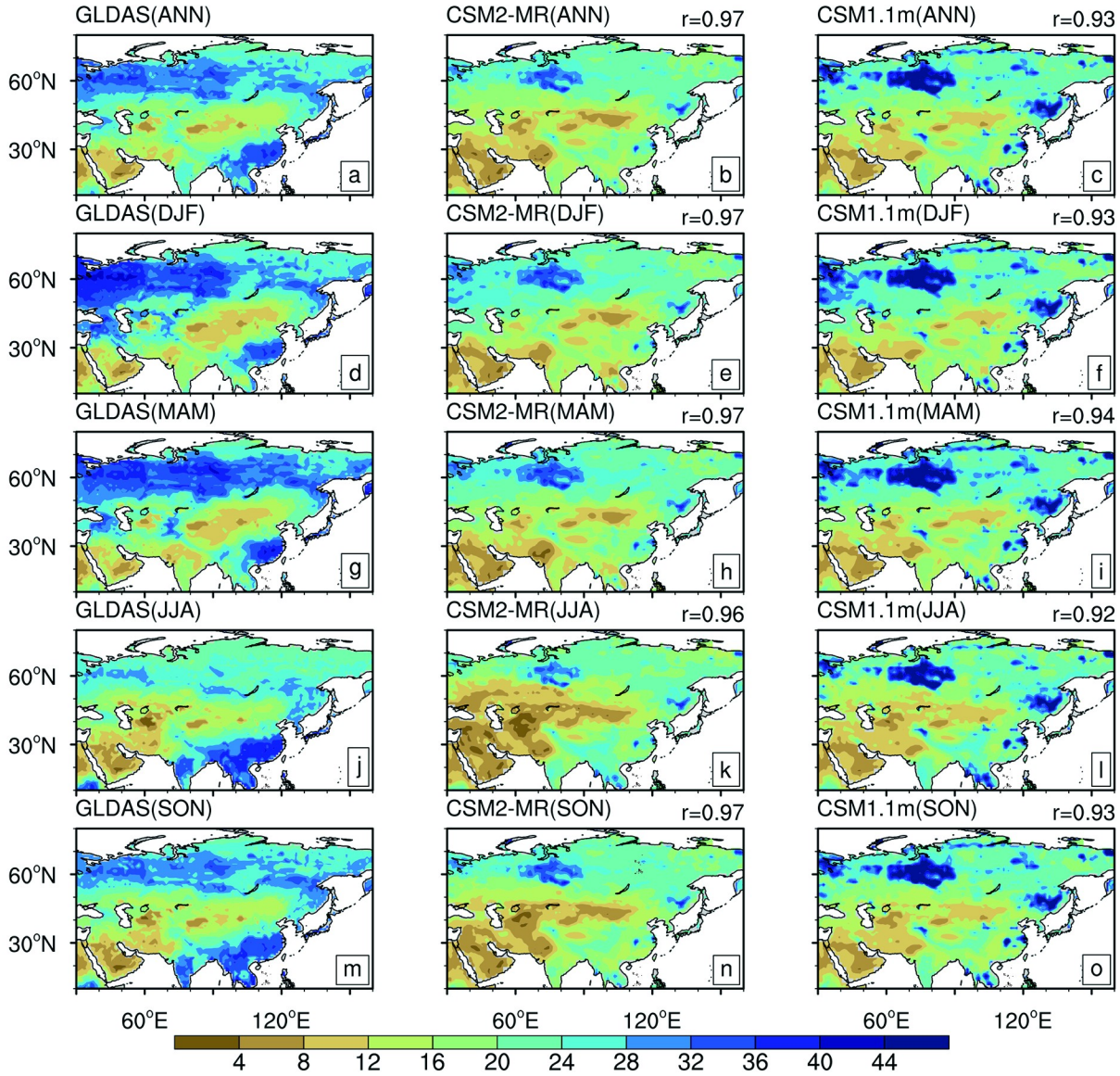

Fig. 1. Climate mean surface soil moisture (units: kg m^{-2}) over Eurasia (1979–2012) on annual and seasonal time scales: (a, d, g, j, m) GLDAS as the reference data; (b, e, h, k, n) BCC-CSM2-MR and the pattern correlation coefficients with GLDAS; (c, f, i, l, o) BCC-CSM1.1m and the pattern correlation coefficients with GLDAS.

between the BCC model simulations and GLDAS in terms of their annual mean and the different seasons are shown in Fig. 2. As the first two columns of the figure show, BCC-CSM2-MR and BCC-CSM1.1m both tend to reproduce soil that is drier than in GLDAS over the whole of Eurasia, with a large coverage of negative values, especially in southern China. Underestimations of SM in climate models have been demonstrated in many previous studies. For example, Ramillien et al. (2003) indicated that Land Dynamics hydrological model tends to underestimate the absolute water storage in the soil and provide smoother values than in-situ measurements. However, in several regions (Siberia, Northeast China, the Yangtze–Huaihe River basin, etc.), the results of the BCC-CSMs tend to be significantly wetter than those of GLDAS. Comparing Figs. 2a and b, we can see that the areas and absolute values of most regions with large differences have reduced from BCC-CSM1.1m to BCC-CSM2-MR in terms of their annual mean. Taking the positive value in Siberia as an example, the SM difference between BCC-CSM1.1m and GLDAS is greater than 20 kg m^{-2}. However, it decreases to around 5 kg m^{-2} in BCC-CSM2-MR, with obvious improvement. This is also the case in the four seasons. Furthermore, compared to the previous-generation model, the RMSE values of BCC-CSM2-MR are lower both in terms of their annual mean and in the four seasons. The mean RMSE of the climate mean state declines by 7.5% from 9.37 (BCC-CSM1.1m) to 8.67 (BCC-CSM2-MR), which demonstrates that BCC-CSM2-MR is more capable of describing the actual distribution of the climate mean surface SM, with fewer biases. The differences between BCC-CSM2-MR and BCC-CSM1.1m are shown in the rightmost panel of Fig. 2. Clear improvements can be seen in Siberia,

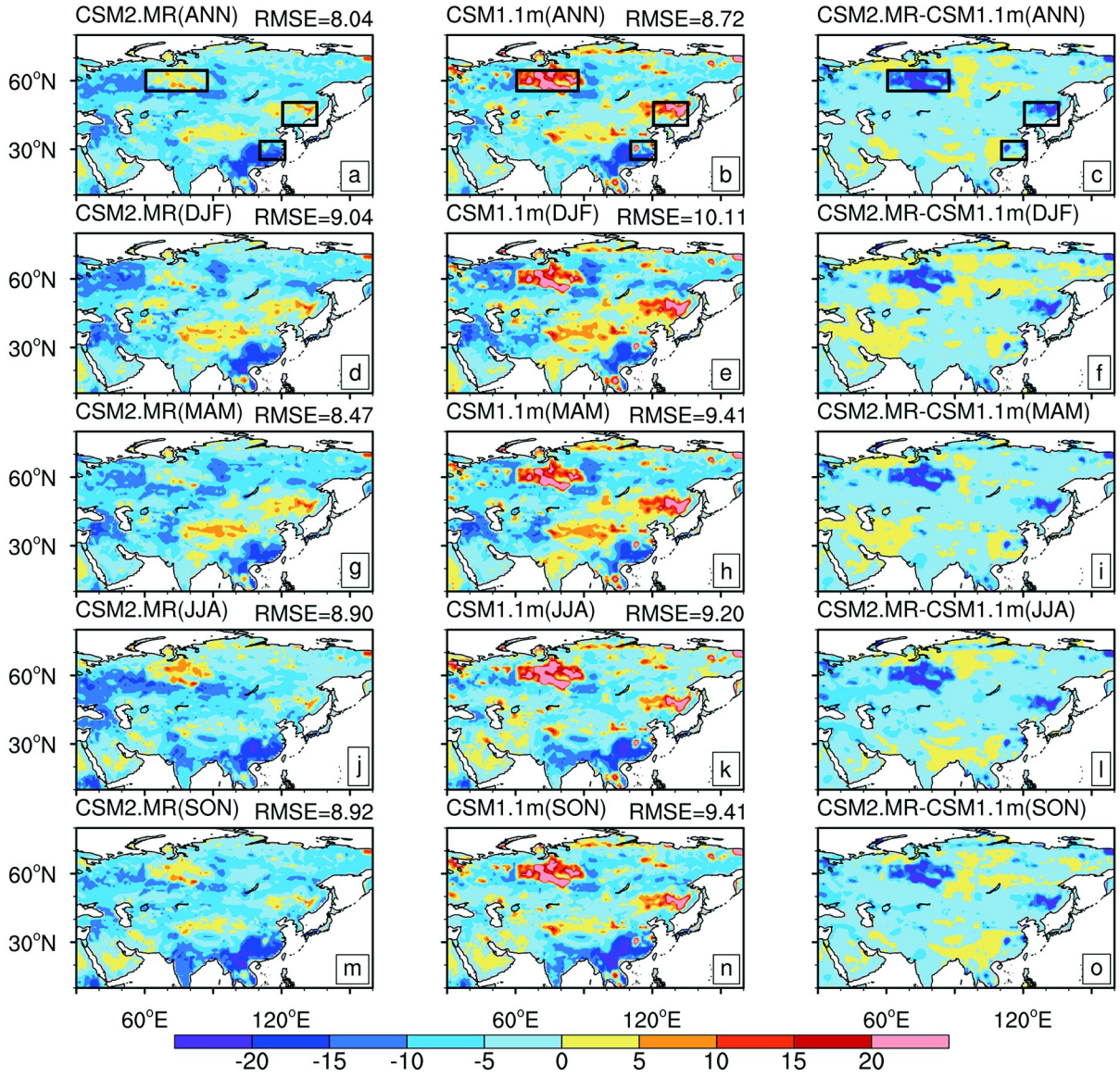

Fig. 2. Differences in climate mean surface soil moisture (units: kg m^{-2}) between GLDAS and BCC simulations on annual and seasonal time scales: (a, d, g, j, m) differences and RMSEs between GLDAS and BCC-CSM2-MR; (b, e, h, k, n) differences and RMSEs between GLDAS and BCC-CSM1.1m; (c, f, i, l, o) differences between BCC-CSM2-MR and BCC-CSM1.1m.

Northeast China, and the Yangtze–Huaihe River basin, which are basically the same as the areas of large BCC model–GLDAS differences mentioned above.

Figure 3 compares the standard deviations of the climate mean surface SM over Eurasia in terms of their annual mean and in the different seasons between the BCC model simulations and the GLDAS data. GLDAS shows that the larger standard deviations tend to be found at high latitudes and in part of central Asia, and clearly during winter and spring (Figs. 3d and g). This illustrates that the surface SM over these regions varies greatly and is spread out over a wider range in winter and spring. Conversely, the variations of surface SM in the low–middle latitudes are quite small, as illustrated by the relatively lower standard deviations over these areas. Gu et al. (2019) indicated that significantly lower SM is generally found in Russia and northeastern Asia, which are similar to the areas with large variations in Figure 3. It appears that both BCC-CSM2-MR and BCC-CSM1.1m are able to capture the spatial patterns, except that the amplitudes of variation are relatively weaker than in GLDAS. For instance, the standard deviation over western Siberia during winter is supposed to exceed 6 kg m^{-2} (Fig. 3d), but the simulated values in the BCC models range between 4 kg m^{-2} and 5 kg m^{-2}. Despite the underestimations to a certain extent, BCC-CSM2-MR has made progress in terms of the standard deviation distributions, with higher pattern correlation coefficients than BCC-CSM1.1m in the annual mean and most seasons. The average pattern correlation coefficient increases by 4%, from 0.81 to 0.84. Therefore, BCC-CSM2-MR is better at describing the variations

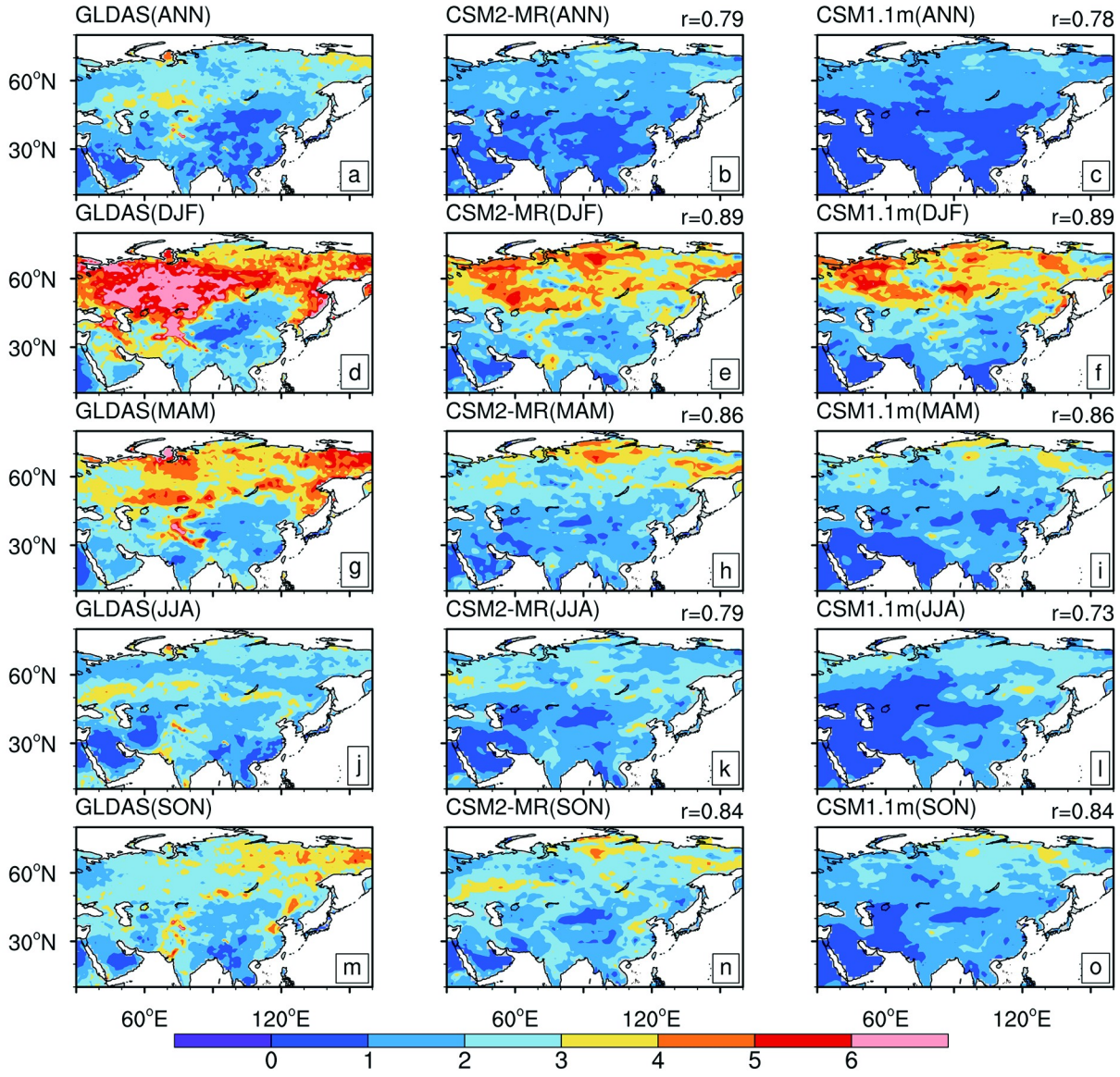

Fig. 3. Standard deviations of climate mean surface soil moisture on annual and seasonal time scale: (a, d, g, j, m) GLDAS as the reference data; (b, e, h, k, n) BCC-CSM2-MR and the pattern correlation coefficients of standard deviations with GLDAS; (c, f, i, l, o) BCC-CSM1.1m and the pattern correlation coefficients of standard deviations with GLDAS.

of surface SM.

We also calculate the differences of the aforementioned standard deviations over Eurasia. Although the difference patterns between BCC-CSM2-MR and GLDAS are similar to those between BCC-CSM1.1m and GLDAS in terms of their annual mean (Figs. 4a and b), the discrepancies of BCC-CSM2-MR are less significant than those of BCC-CSM1.1m in the four seasons, especially in western Siberia and central Asia during spring, summer and winter, because the areas and absolute negative values decrease. That is to say, there is a certain underestimation in BCC-CSM1.1m when describing the standard deviations of SM. In addition, BCC-CSM2-MR is more skillful than BCC-CSM1.1m in terms of RMSE. The RMSE values of BCC-CSM2-MR are distinctly lower than those of BCC-CSM1.1m in terms of their annual mean and all seasons. The average RMSE reduces by 15.6%, from 1.56 to 1.35. This demonstrates that BCC-CSM2-MR is more capable of describing the spatial distributions of surface SM standard deviations, with fewer biases. From the rightmost panel of Fig. 4, we can see that the reason for the better performances in BCC-CSM2-MR is that the standard deviations described in BCC-CSM2-MR are systematically greater than those in BCC-CSM1.1m. This overcomes the defect of the underestimation in the previous generation, hence allowing BCC-CSM2-MR to present the degree of surface SM variation more accurately, especially in the middle and high latitudes.

To make the results of the comparison more robust, we also employ a station-based observational SM dataset in China as the reference data. Due to the relatively greater number of missing values in the cold seasons, Fig. 5 only shows the difference patterns of the climate mean SM and the distri-

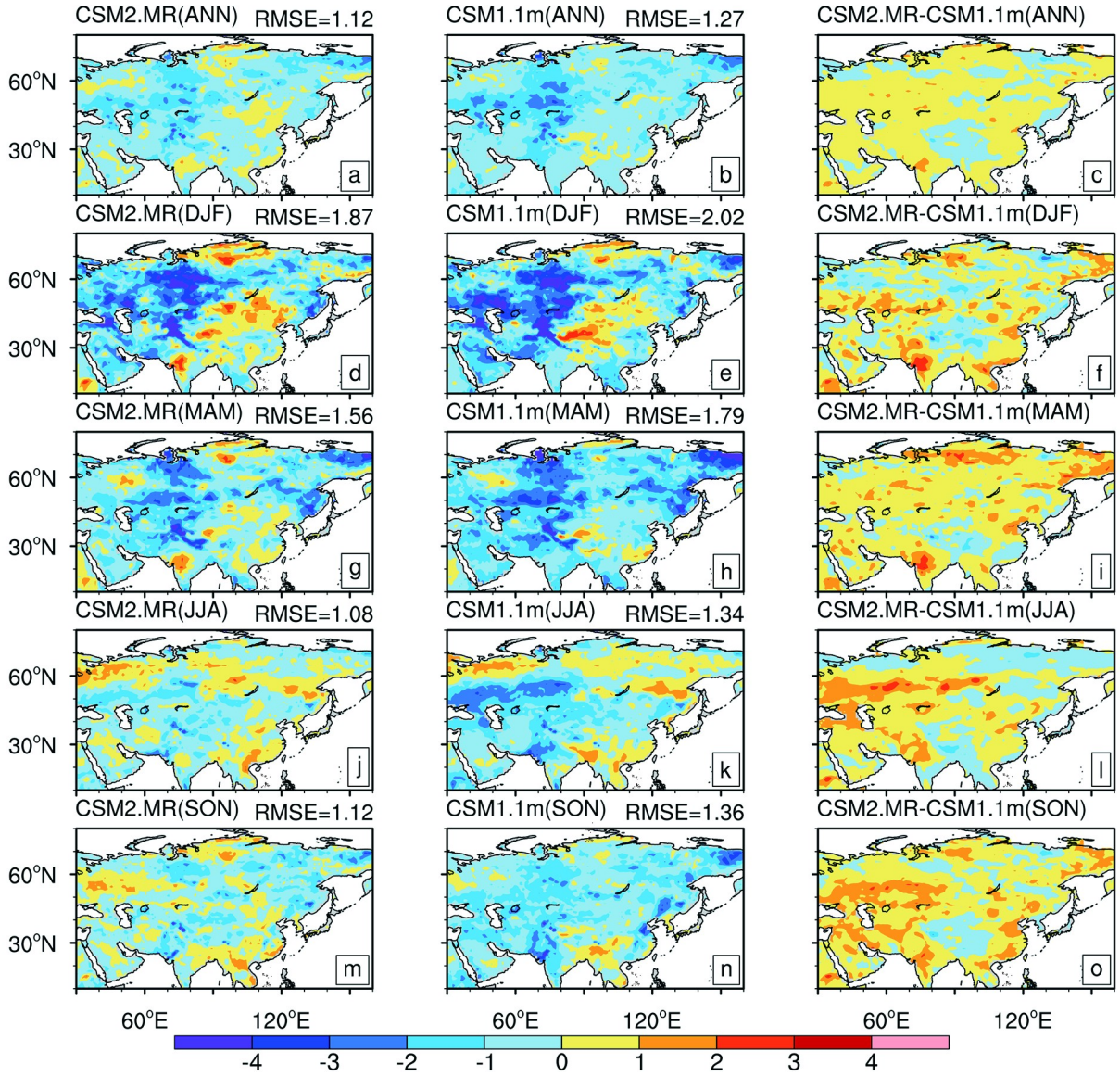

Fig. 4. Differences in standard deviations of mean surface soil moisture between GLDAS and model simulations on annual and seasonal times scales: (a, d, g, j, m) differences and RMSEs between GLDAS and BCC-CSM2-MR; (b, e, h, k, n) differences and RMSEs between GLDAS and BCC-CSM1.1m; (c, f, i, l, o) differences between BCC-CSM2-MR and BCC-CSM1.1m.

butions of the standard deviations in summer; the results of the annual mean and other seasons are listed in Tables 2 and 3. From Figs. 5a and b, we can see that the SM over the Yangtze–Huaihe River basin and Northeast China simulated by BCC-CSM1.1m is obviously wetter than observed, but this situation improves in BCC-CSM2-MR. Figure 5c shows that through revising the overestimations over the regions mentioned above in the previous generation, the biases of the climate mean SM relative to observations are less severe in BCC-CSM2-MR. The reduction in RMSE (from 10.92 to 9.62) also demonstrates that the ability of the model simulation has been improved. It is worth noting that the patterns shown in Figs. 5a–c are consistent with the patterns in Fig. 2, where the reference data are from GLDAS. Figures 5d and e show that both BCC-CSM1.1m and BCC-CSM2-MR can capture the pattern of variation in SM over North China as being larger than in other areas, but the amplitudes are smaller than those of the observations to different degrees. However, BCC-CSM2-MR (standard deviation: 2.04) still performs better than BCC-CSM2-MR (standard deviation: 1.63), based on the closer average standard deviation to that of the observations (standard deviation: 3.22). The simulations of BCC-CSM2-MR in terms of the annual mean and the other seasons are also improved (Tables 2 and 3).

3.1.2. *EOF analysis*

The spatial features of surface SM anomalies over Eurasia from 1979 to 2012 are analyzed by using the EOF method. Figure 6 displays the first two principle compon-

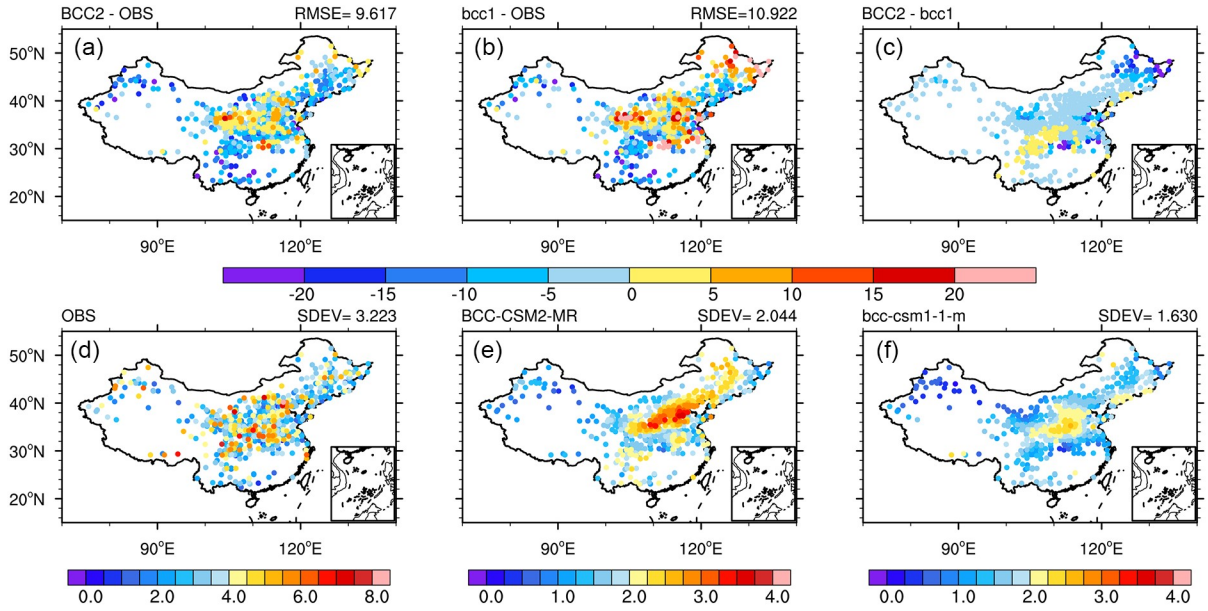

Fig. 5. Differences in climate mean surface soil moisture between observations and BCC simulations over China in summer and the standard deviations of three datasets: (a–c) differences and RMSEs; (d–f) standard deviations.

Table 2. RMSEs between observations and the BCC models in terms of climate-mean SM.

	Annual	DJF	MAM	JJA	SON
BCC-CSM2-MR	11.04	13.04	9.21	9.62	10.71
BCC-CSM1.1m	13.21	14.63	11.16	10.92	12.53

Table 3. Mean standard deviations of the observed and BCC-modeled SM.

	Annual	DJF	MAM	JJA	SON
Observations	1.99	3.40	3.17	3.22	3.44
BCC-CSM2-MR	0.97	1.77	1.59	2.04	1.84
BCC-CSM1.1m	0.77	1.39	1.13	1.63	1.44

ents of the EOF analysis of GLDAS and the BCC model simulations. The EOF1 pattern in GLDAS, which explains 34.1% of the variance (Fig. 6a), shows that there are significant negative signals in the western Siberia, central Asia and the Kamchatka region, while other areas in Eurasia are covered by weak positive signals. This pattern suggests that the surface soil tends to getting drier in western Siberia, central Asia and Kamchatka region, but slightly wetter in other areas. In the EOF2 pattern of GLDAS, with an explained variance of 8.9% (Fig. 6b), there is a large-scale drying trend at high latitudes and mild wetting trend in other areas. The results are consistent with previous studies (Dong et al., 2007; Cheng et al., 2015; Gu et al., 2019). In BCC-CSM2-MR, the explained variance of the first two principle components reaches 20.0% in total (Figs. 6d and e). The EOF1 pattern of BCC-CSM2-MR that can capture negative values in western Siberia and central Asia has relatively high similarity with the EOF1 pattern of GLDAS. However, there are still some disagreements between BCC-CSM2-MR and GLDAS in the first principle component over the Arctic coastal region. This area is covered by positive values in BCC-CSM2-MR, which means the surface SM there tends to be wet. This trend is opposite to that of GLDAS. Therefore, BCC-CSM2-MR is able to capture the EOF1 spatial pattern of GLDAS, except at high latitudes in Arctic coastal regions. The EOF2 pattern of BCC-CSM2-MR, which shows that large-scale negative values cover the high latitudes, is similar to that of GLDAS, except that the gradient is not as obvious as shown in GLDAS. As for BCC-CSM1.1m, EOF1 (Fig. 6g) is unable to capture the spatial pattern of drying at high latitudes, as shown in the EOF1 of GLDAS and BCC-CSM2-MR. Neither western Siberia nor the Kamchatka region has the signs of a drying trend of surface SM. In the EOF2 pattern of BCC-CSM1.1m (Fig. 6h), the high latitudes are covered by negative values, but their area and gradient are relatively smaller. In conclusion, compared to the previous-generation model, BCC-CSM2-MR is more skillful in describing the first two principle components of the EOF analysis of the surface SM anomaly over Eurasia from 1979 to 2012. The periodogram estimates of the spectra of the first principal component time series (PC1) of GLDAS and the BCC model simulations are shown in the rightmost column of Fig. 6. The spectra above the red line are approved by the Markov "red noise" test. As shown in the panel, the corresponding period of GLDAS PC1 is 16.6 years. For the PC1s of BCC-CSM2-MR and BCC-CSM1.1m, the periods are 13.3 years and 8.3 years, respectively. Obviously, the period of PC1 in BCC-CSM2-MR is much closer to that in GLDAS. Therefore, BCC-CSM2-MR is more capable of capturing the periodicity characteristics of the SM variation.

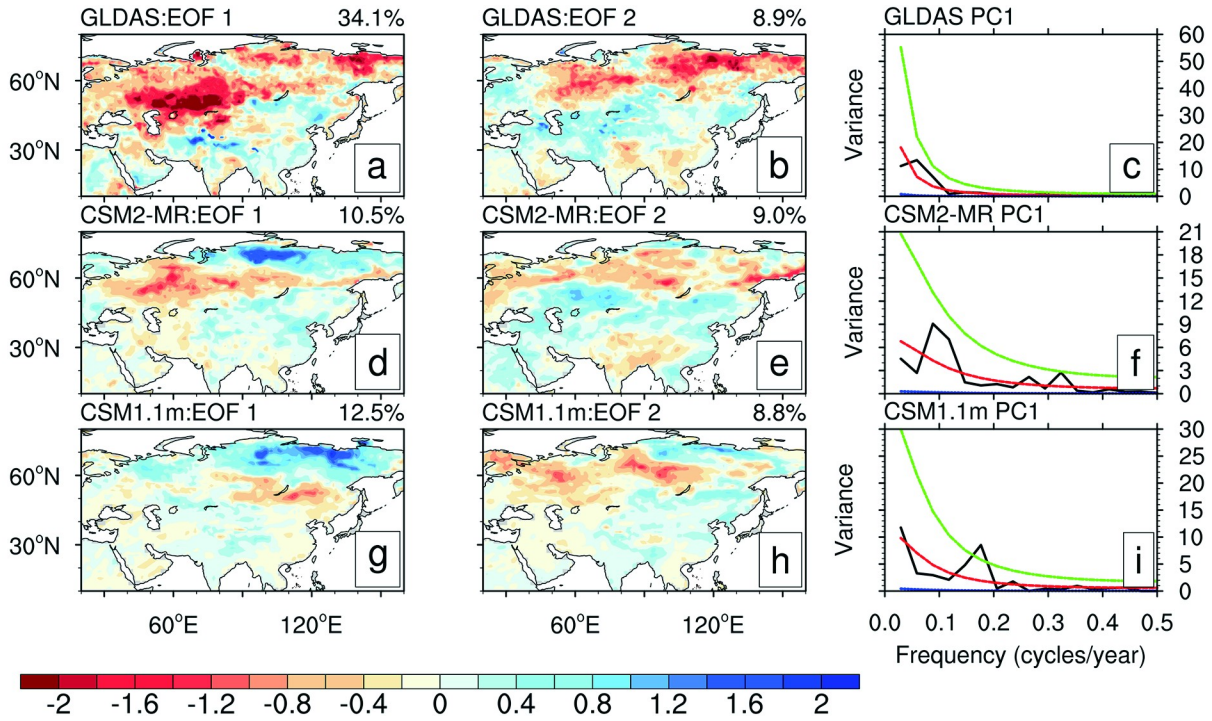

Fig. 6. The first two EOFs of annual mean soil moisture and periodogram estimates of the spectra of the PC1s: (a, d, g) EOF1 for GLDAS, BCC-CSM2-MR and BCC-CSM1.1m, respectively; (b, e, h) EOF2 for GLDAS, BCC-CSM2-MR and BCC-CSM1.1m, respectively; (c, f, i) periodogram estimates of the spectra of the PC1s of GLDAS, BCC-CSM2-MR and BCC-CSM1.1m (red lines: Markov "red noise" spectrum; green lines: upper confidence bound for Markov; blue lines: lower confidence bound for Markov).

3.2. *Evaluation of BCC-CSM2-MR among CMIP6 models*

We also compare the performance of BCC-CSM2-MR over Eurasia and China on annual and seasonal time scales with the other models participating in CMIP6, by using centered pattern correlation (computing anomalies from a central mean) and "amplitude of variations" (relative standard deviation). To make the comparison more comprehensive, BCC-CSM1.1m, the previous-generation model of BCC-CSM2-MR that participated in CMIP5, is also taken into account. Taylor diagrams (Taylor, 2001) are used to provide a visual representation of the aforementioned metrics.

Centered pattern correlations between the surface SM simulated by the models and GLDAS are indicated by the azimuthal position of each dot in the Taylor diagrams. For the simulated annual mean surface SM (Fig. 7a), the dots are relatively scattered. Correlations generally fall between 0.6 and 0.9 and tend to be clustered around 0.7. Compared with other CMIP6 models, BCC-CSM2-MR (r = 0.77), second only to EC-Earth3-Veg (r = 0.83) and MRI-ESM2-0 (r = 0.78), performs at a high level. BCC-CSM2-MR also shows marked progress in correlation compared with BCC-CSM1.1m (r = 0.62), with a rate of increase of 24.2%. In different seasons (Figs. 7b–e), although the correlations between the CMIP6 models and GLDAS are more variable, BCC-CSM2-MR is still well ahead of most models. Especially in winter (Fig. 7b), BCC-CSM2-MR has the highest correlation coefficient with GLDAS (r = 0.77). Also, the coefficients of BCC-CSM2-MR are obviously higher than those of BCC-CSM1.1m in all seasons. The radial distance from the origin represents the standard deviation of the model simulation relative to the standard deviation of GLDAS (σ sim / σ obs). The closer to 1 the ratio is, the fewer biases in simulating SM variations the models have. In terms of the annual mean (Fig. 7a), most models overestimate the standard deviation of surface SM considerably, with ratios above 1.25. BCC-CSM2-MR (σ sim / σ obs = 0.83) is one of the models able to give a comparatively accurate representation of the standard deviation. Meanwhile, compared with BCC-CSM1.1m (σ sim / σ obs = 1.24), BCC-CSM2-MR also does a better job. During different seasons (Figs. 7b–e), the ratios of BCC-CSM2-MR are between 0.77 and 0.88 (the average ratio is 0.81), which places BCC-CSM2-MR at a better level among the CMIP6 models (the average ratio is 1.48) in representing similar standard deviations to GLDAS. However, compared to the previous-generation model, with slight overestimation (average ratio of 1.15), the improvements of BCC-CSM2-MR are not that obvious.

For the area of China, the dots in Fig. 8 are more clustered than in Fig. 7, which means that the models perform relatively consistently over China. For the annual mean surface SM (Fig. 8a), the correlation coefficients in the model simulations fall between 0.4 and 0.8. BCC-CSM2-MR (r = 0.61) is at the mid-upper level among the CMIP6 models. Compared with BCC-CSM1.1m (r = 0.41), BCC-CSM2-MR has made an evident improvement. In the

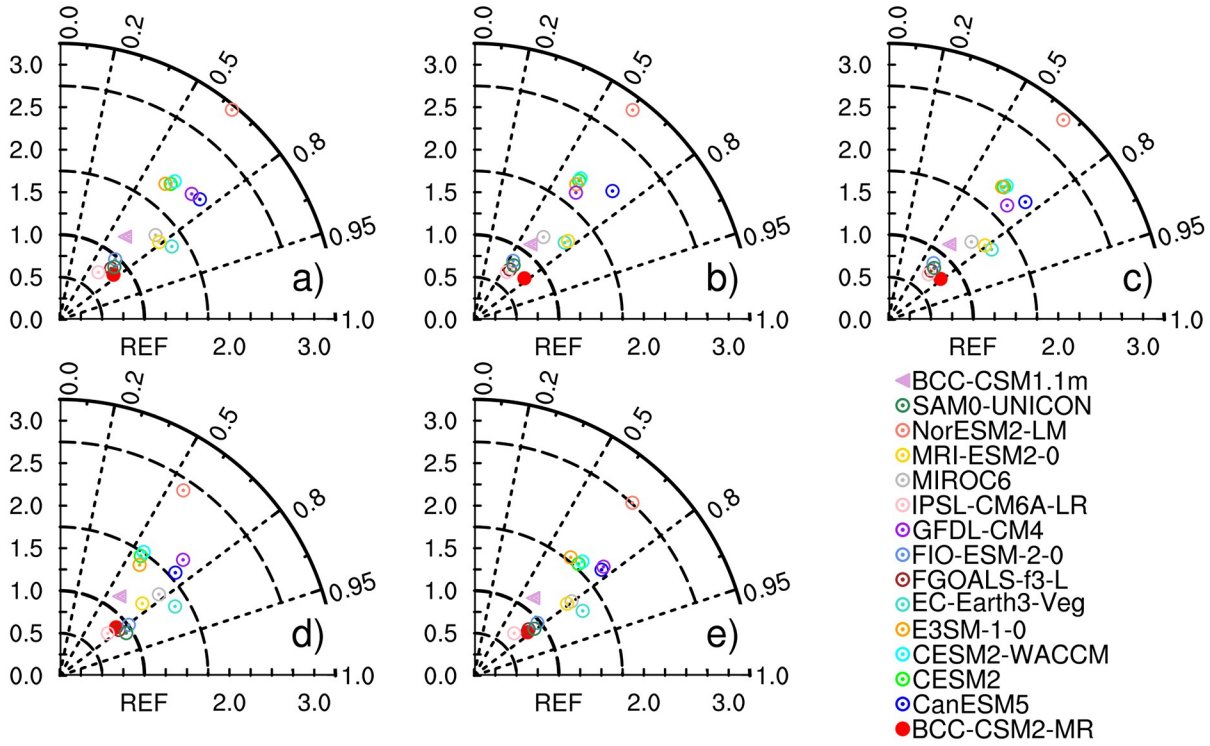

Fig. 7. Taylor diagrams for model-simulated surface soil moisture based on GLDAS over Eurasia: (a) annual mean; (b) winter; (c) spring; (d) summer; (e) autumn.

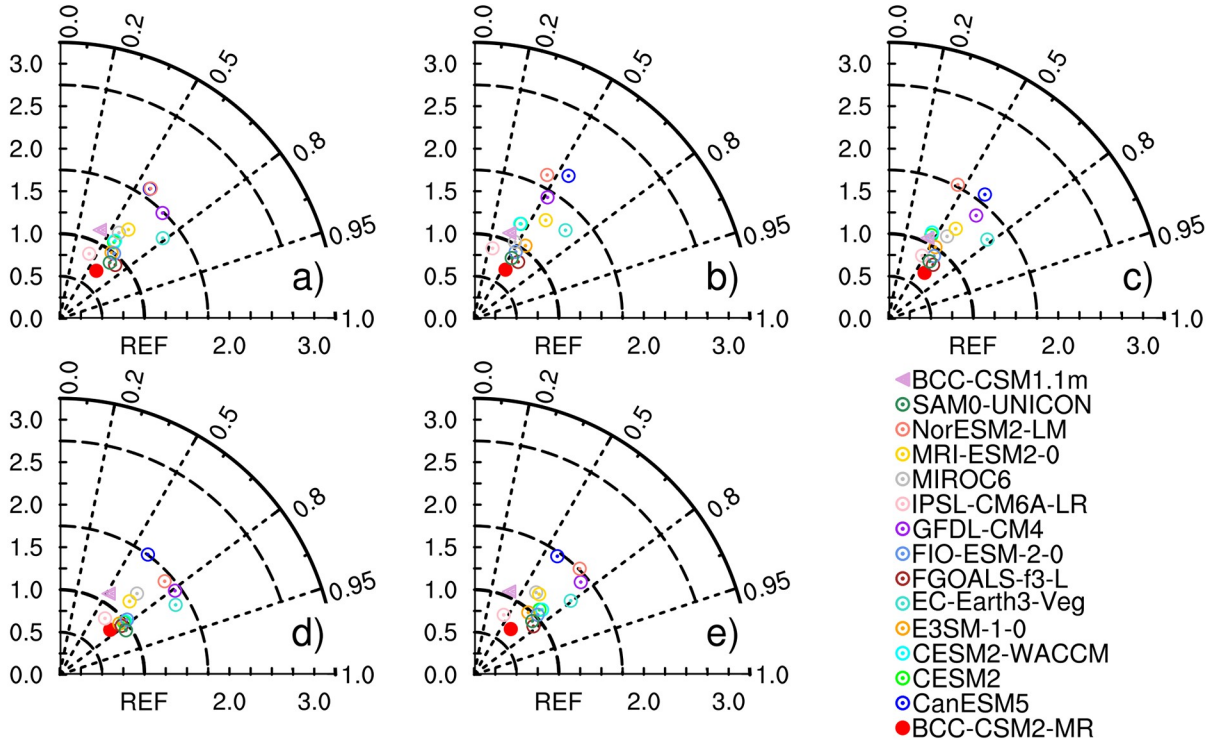

Fig. 8. Taylor diagrams for model-simulated surface soil moisture based on GLDAS over China: (a) annual mean; (b) winter; (c) spring; (d) summer; (e) autumn.

four seasons (Figs. 8b–e), the correlation coefficients of BCC-CSM2-MR always fall within the range of 0.5–0.8. The average is 0.64, which is higher than that of the CMIP6 models ($r = 0.61$), showing BCC-CSM2-MR to be more skillful in accurately and consistently representing the distribution of surface SM compared to most of the CMIP6 models.

Meanwhile, BCC-CSM2-MR takes the lead in comparison with BCC-CSM1.1m (average correlation coefficient is 0.40). As for the ratios between the standard deviations of the model simulations and those of the reference data, the advantages of BCC-CSM2-MR are highlighted. The ratios of BCC-CSM2-MR are generally around 0.7–0.8 which are the closest to 1 among all the CMIP6 models. This indicates that BCC-CSM2-MR can capture the variability of the surface SM properly and maintain a minimum bias relative to the reference data. Compared with BCC-CSM1.1m, BCC-CSM2-MR carries forward the advantage of a similar standard deviation to that of GLDAS, and a slight improvement to the overestimation of the previous-generation model.

In general, compared with other CMIP6 models and BCC-CSM1.1m, BCC-CSM2-MR is more competent in describing the distributions and variations of annual and seasonal SM, as shown by the relatively higher centered pattern correlation and standard deviation that is closer to that of the reference data, either in Eurasia or China.

3.3. *Role of precipitation in soil moisture simulation*

The above analysis shows that BCC-CSM2-MR has made certain progress in the simulation of surface SM compared to BCC-CSM1.1m. This might benefit from improvements to parameterization schemes in the component models, especially the land model implemented in BCC-CSM2-MR (Wu et al., 2019), such as the inclusion of a variable temperature threshold to determine soil water freeze–thaw, rather than a fixed temperature of 0 °C, a better calculation of snow cover fraction, and so on (Li et al., 2019). In the actual process of land–atmosphere coupling, there are many elements that have effects on the variations of SM, such as precipitation, temperature, wind, etc. Among these elements, precipitation is well known as the most vital and has thus been widely studied. The wetting of soil by precipitation, identified as the first part of the land–atmosphere feedback of water, is straightforward and intuitive and indisputably occurs in nature (Koster et al., 2003, 2004; Tawfik and Steiner, 2011). Numerous studies have shown that precipitation is the most direct and vital among the factors affecting SM. Zhang et al. (2008) used analysis data of precipitation and SM from GLDAS and pointed out that the strong land–atmosphere coupling lies mainly in semi-humid forest to grassland transition zones or in arid to semi-arid transition zones, including central Eurasia, northern China, etc. Research has also shown that the interaction between precipitation and SM exists in atmospheric general circulation models (Oglesby and Erickson III, 1989; Dirmeyer, 2000).

The SM procedure adopted in BCC-CSM is almost the same as that in the NCAR Community Land Model (Oleson et al., 2004). SM is governed by infiltration, surface and sub-surface runoff, gradient diffusion, gravity, and root extraction through canopy transpiration. For one-dimensional vertical water flow in soils, the conservation of mass is stated as

$$\frac{\partial \theta}{\partial t} = -\frac{\partial q}{\partial z} - e, \tag{1}$$

where θ is the volumetric soil water content, t is time and z is height above some datum in the soil column, q is the soil water flux, and e is the evapotranspiration loss. In the coupling between the land model and atmospheric model, liquid and solid precipitation from the atmospheric model will have an important effect on q and subsequently influence the simulation of SM. Therefore, the improvements in SM simulation in BCC-CSM2-MR may be attributable to a better simulation of precipitation. Influences of precipitation on SM in the models are thus discussed as follows.

Differences in the climate mean of the surface SM (c.f. Fig. 2) have shown that there are three regions where the difference values are significantly improved: Siberia (55°–64°N, 60°–87°E), Northeast China (40°–50°N, 120°–135°E), and the Yangtze–Huaihe River basin (28°–33°N, 110°–121°E). The difference values in these three regions decrease by 32.7%, 30.0% and 20.6%, respectively. Hence, we select these three subregions (see the black sectors in Figs. 2a–c) and the whole of Eurasia as target areas to investigate the possible reasons behind the improvement in SM simulation, which has been linked with precipitation.

Figure 9 shows the correlation coefficients between the time series of the annual mean surface SM and precipitation in the reference data (GLDAS for SM, CMAP for precipitation) and the BCC model simulations. In GLDAS/CMAP, the correlation coefficients range between 0.35 and 0.60, which are statistically significant at the 95% confidence level according to the Student's t-test. As for the BCC model simulations, the correlation coefficients are generally significant in most areas except the whole of Eurasia. For Eurasia, which of course covers a wide range of longitudes and latitudes, the factors that influence SM in are more complex and diverse. Therefore, this complicated land–atmosphere interaction makes the proportion of the influence of precipitation on SM smaller and the correlation coefficients

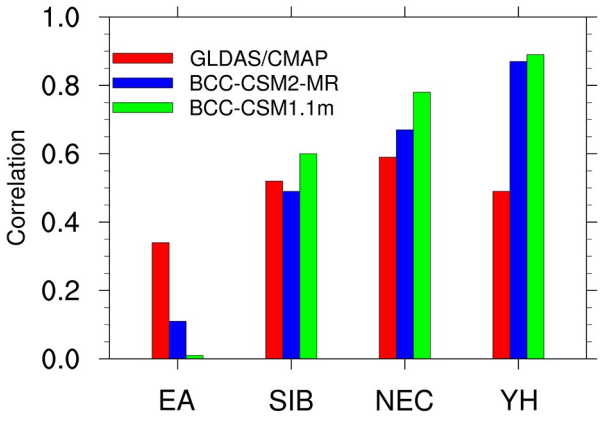

Fig. 9. Correlation coefficients between the annual mean time series of soil moisture and precipitation of BCC-CSM2-MR, BCC-CSM1.1m and reference data (GLDAS/CMAP) over Eurasia (EA), Siberia (SIB), Northeast China (NEC) and the Yangtze–Huaihe River basin (YH).

between them to be reduced further. Coupled climate models may not properly capture the complicated relationships between SM and factors of influence, and perhaps may even weaken the influence of precipitation excessively. Hence, the correlation coefficients in the BCC model simulations are quite low and even non-significant. As for the three subregions, the correlation coefficients of BCC-CSM2-MR in Siberia, Northeast China and the Yangtze–Huaihe River basin are 0.49, 0.67 and 0.87, respectively, while those of BCC-CSM1.1m are 0.60, 0.78 and 0.89, respectively. The former is apparently lower than the latter and much closer to the coefficients in GLDAS\CMAP (r = 0.52, 0.59 and 0.49, respectively). That is to say, the proportion of influence of precipitation on surface SM in BCC-CSM2-MR is not as much as in BCC-CSM1.1m. As seen on the annual time scale, the coefficients of BCC-CSM2-MR are more consistent with those of the reference data on the seasonal scale (not shown here). In other words, compared with the previous-generation model, BCC-CSM2-MR is able to represent, relatively realistically, the relationship between precipitation and surface SM in these three subregions.

The anomalies of surface SM in GLDAS and the BCC models, in conjunction with corresponding anomalies of precipitation in CMAP and the BCC models, over Eurasia and the three subregions, are shown in Fig. 10. In Eurasia, the SM responses in GLDAS are positively correlated with the precipitation variations in CMAP (Fig. 10a). By analyzing the slope of the regression line, we can conclude that BCC-CSM2-MR is able to represent the correlation with a positive linear regression coefficient, but BCC-CSM1.1m shows

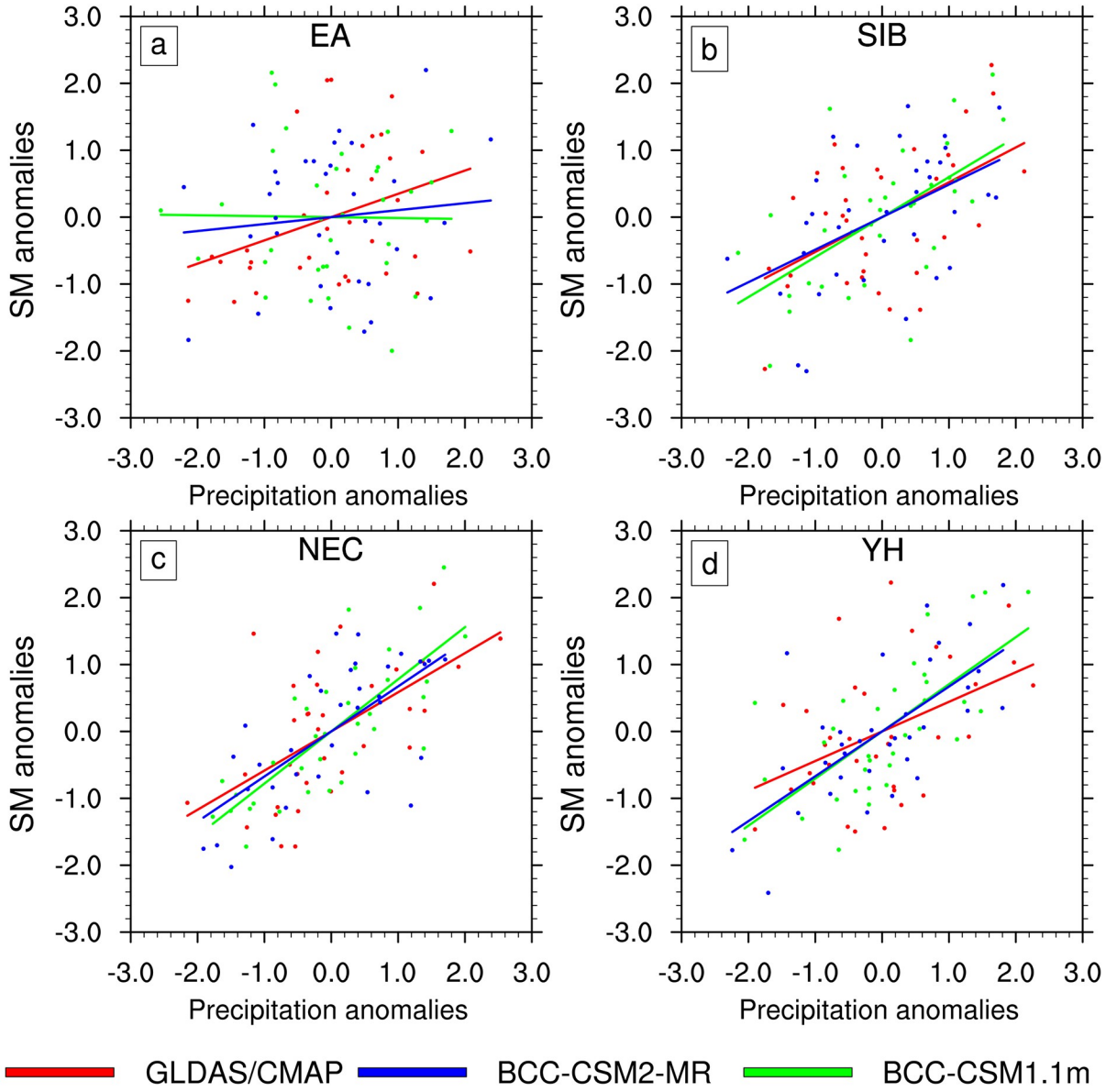

Fig. 10. Scatterplots showing the anomalies of soil moisture in the reference data and BCC models, in conjunction with corresponding changes in precipitation, over (a) Eurasia (EA), (b) Siberia (SIB), (c) Northeast China (NEC) and (e) the Yangtze–Huaihe River basin (YH).

an opposite correlation with a negative linear regression coefficient. In the three subregions (Figs. 10b–d), the dots are not as spread as they are in Eurasia. This means that precipitation anomalies play a more obvious and important role in increasing SM. In general, the regression lines in BCC-CSM2-MR are closer to those in the reference data, as indicated by the similar spacing and trends of the dots. Taking Northeast China as an example, the linear regression coefficient of GLDAS\CMAP is 0.58, while the coefficients of BCC-CSM2-MR and BCC-CSM1.1m are 0.67 and 0.77, respectively. Obviously, the former is closer than the latter to the reference data. Therefore, compared to the previous version, BCC-CSM2-MR is more skillful in describing the relationship between precipitation and surface SM variations.

We also evaluate the RMSE values of the mean precipitation between CMAP and the BCC model simulations on the annual time scale (Table 4). The RMSEs of BCC-CSM2-MR are lower than those of BCC-CSM1.1m to some extent. For Eurasia, the RMSE of the annual mean decreases by 9.6%, from 1.14 (BCC-CSM1.1m) to 1.03 (BCC-CSM2-MR). In the three subregions, the RMSEs of BCC-CSM2-MR tend to be obviously lower. The Yangtze–Huaihe River basin is the region with the most obvious improvement, where the RMSE is reduced by 40.4%. The progress is also significant on the seasonal time scale (not shown here). Hence, BCC-CSM2-MR is generally more skillful than BCC-CSM1.1m in realistically representing the variation of precipitation, as shown by the smaller deviation between the simulation and CMAP.

From the above analyses, BCC-CSM2-MR is better able to properly describe the correlation between the surface SM and precipitation, the response of the surface SM variation to precipitation anomalies, and the variation of precipitation. These qualities may contribute to the better simulation of surface SM in BCC-CSM2-MR.

4. Summary and discussion

This study has evaluated the surface SM simulations of BCC-CSM2-MR over Eurasia on annual and seasonal time scales and compared them with its previous-generation version (BCC-CSM1.1m) and other CMIP6 models, as well as with GLDAS and station-based observations as reference data, and further discussed the possible reasons behind the improvement in surface SM simulations in relation to precipitation. The conclusions can be summarized as follows:

BCC-CSM2-MR, which is participating in CMIP6, has clearly improved SM simulations compared with BCC-CSM1.1m, part of CMIP5, not only in terms of spatial distributions of the climate mean surface SM, with higher pattern correlations with GLDAS, but also in terms of obviously reduced RMSEs. The standard deviations of BCC-CSM2-MR also have closer spatial distributions to those of the reference data, and the RMSEs are generally lower. The first two principle components of BCC-CSM2-MR are able to capture the spatial patterns shown as EOF1 and EOF2 of GLDAS, while BCC-CSM1.1m struggles to describe the characteristics properly. Compared with the 8.3-year period of PC1 shown in BCC-CSM1.1m, the period in BCC-CSM2-MR (13.3 years) is closer to that in GLDAS (16.6 years).

Among the other models participating in CMIP6, BCC-CSM2-MR performs well in statistical diagnostics. The average centered correlation coefficient of BCC-CSM2-MR (r = 0.77) is the third highest among the CMIP6 models. The average relative standard deviation is 0.83, closer to that of the reference data, which surmounts the overestimations in most of the CMIP6 models.

The possible reasons behind the improvement in BCC-CSM2-MR, as related to precipitation, have been discussed. BCC-CSM2-MR simulates correlation coefficients and regression coefficients that are closer to those of GLDAS\CMAP. The simulation of precipitation by BCC-CSM2-MR is also improved in terms of the RMSE.

In addition to the above conclusions, we found that the improvement of BCC-CSM2-MR differs from season to season. Specifically, the performances in autumn and winter are better than in spring and summer. Taking the simulations of the climate mean SM for example, the pattern correlation coefficient between model and reference data increases by 4.3%, from 0.93 to 0.97, in autumn and winter, which is higher than that the rate of 3.7% in spring and summer. The reduction in RMSE is 8.0% in autumn and winter, while it is 6.6% in spring and summer. The different performances between the cold and warm seasons are possibly related to the optimization of parameterization schemes. In BCC_AVIM1.0 (the land component in BCC-CSM1.1m), liquid water freezes when the soil temperature decreases to 0°C, and the soil temperature will remain at 0°C until all the liquid water has frozen. However, liquid water can coexist with ice in the real world when the soil temperature is below 0°C. The relationship between soil water content and soil temperature is determined by the inherent characteristics of soil hydraulics and the thermodynamic equilibrium between soil water potential and soil temperature. Therefore, the method to calculate the soil freeze–thaw critical temperature used by Li and Sun (2008) is adopted in BCC_AVIM2.0 (the land component in BCC-CSM2-MR) to replace the unreasonable assumption used in BCC_AVIM1.0. In addition, the parameterization of snow cover fraction in BCC_AVIM2.0 is also adjusted for the

Table 4. RMSEs between the BCC models and CMAP data of annual mean precipitation over Eurasia and four subregions.

	Eurasia (10°–80°N, 30°–160°E)	Siberia (55°–64°N, 60°–87°E)	Northeast China (40°–50°N, 120°–135°E)	Yangtze–Huaihe River basin (25°–33°N, 110°–121°E)
BCC-CSM2-MR	1.03	0.24	0.36	0.81
BCC-CSM1-1-m	1.14	0.28	0.47	1.36

absence of fluctuating topography by taking into account the subgrid variability of topography in a model grid cell (Li et al., 2019). Thus, the optimization for the parameterization schemes of soil freeze–thaw processes and the snow cover fraction may result in BCC-CSM2-MR performing better in its autumn and winter season simulations.

Also of note is that the performance of BCC-CSM2-MR improves differently in different regions. Possible reasons related to parameterization schemes are discussed here. In Fig. 2, the areas with significant improvement are mostly located in Eurasian mid–high latitudes (Siberian region and Northeast China). For the relatively higher latitudes, processes related to snow cover and soil water freeze–thaw are more significant and important than in the low latitudes. Therefore, the upgrading of related parameterization schemes mentioned above will make more obvious improvements in the high latitudes. It is worth noting that the Yangtze–Huaihe River basin is also an area showing significant improvement. This area is the main rice production region in China. The interactions between such agricultural land and the overlying atmosphere play an important role, where surface latent heat flux values are relatively large. However, the plant functional type of "crop" in BCC_AVIM1.0 to represent rice paddies will underestimate the amount of surface evaporation, which is the important link between SM and the atmosphere. A new scheme for rice paddy fields was developed in BCC_AVIM2.0 to incorporate the addition of surface water above soil (Li et al., 2019). The essential difference in the calculation of latent heat flux between BCC_AVIM2.0 and the original crop scheme in BCC_AVIM1.0 lies in that there is no limit to the evaporation from a rice paddy in BCC_AVIM2.0. Therefore, the optimization of the parameterization over rice paddies may result in the model improvement in the Yangtze–Huaihe River basin.

However, there are still some limitations in this study. First, we applied bilinear interpolation to regrid both the simulation data and reference data into a uniform resolution of 1° × 1° to make the evaluation more convenient, which might have affected the conclusions to a certain degree because of the inhomogeneity of SM. Although bilinear interpolation is a simple method and commonly used (Crow et al., 2012; Hsu et al., 2013; Yuan and Quiring, 2017), applying a more advanced downscaling or interpolation technique may provide better estimates of model-simulated SM. Second, this study has only discussed the correlation between SM and precipitation. In fact, the improvements in related land surface process schemes are also important, as well as the land–atmosphere coupling in other component models, and so precipitation is merely one of the most-related factors. Other factors need more and further investigations in the future.

Acknowledgements. This work was supported by the National Key Research and Development Program of China (Grant Nos. 2018YFC1506004 and 2016YFA0602602).

REFERENCES

Berg, A., and J. Sheffield, 2018: Soil moisture-evapotranspiration coupling in CMIP5 models: Relationship with simulated climate and projections. *J. Climate*, **31**, 4865–4878, https://doi.org/10.1175/JCLI-D-17-0757.1.

Cheng S. J., X. D. Guan, J. P. Huang, and M. X. Ji, 2013: Analysis of response of soil moisture to climate change in semi-arid loess plateau in China based on GLDAS data. *Journal ofAridMeteorology*,**31**(4),641–649,https://doi.org/10.11755/j.issn.1006-7639(2013)-04-0641. (in Chinese with English abstract)

Cheng, S. J., X. D. Guan, J. P. Huang, F. Ji, and R. X. Guo, 2015: Long-term trend and variability of soil moisture over East Asia. *J. Geophys. Res.*, **120**, 8658–8670, https://doi.org/10.1002/2015JD023206.

Crow, W. T., and Coauthors, 2012: Upscaling sparse ground-based soil moisture observations for the validation of coarse-resolution satellite soil moisture products. *Rev. Geophys.*, **50**, RG2002, https://doi.org/10.1029/2011RG000372.

Dai, C. Y., and Z. Y. Zuo, 2010: Relationship between previous winter and spring soil moisture and summer climate in eastern China. *Meteorological Science and Technology*, **38**(3), 300–305, https://doi.org/10.19517/j.1671-6345.2010.03.005. (in Chinese with English abstract)

Dirmeyer, P. A., 2000: Using a global soil wetness dataset to improve seasonal climate simulation. *J. Climate*, **13**, 2900–2922, https://doi.org/10.1175/1520-0442(2000)013<2900:UAGSWD>2.0.CO;2.

Dirmeyer, P. A., C. A. Schlosser, and K. L. Brubaker, 2009: Precipitation, recycling, and land memory: An integrated analysis. *Journal of Hydrometeorology*, **10**, 278–288, https://doi.org/10.1175/2008JHM1016.1.

Dirmeyer, P. A., Y. Jin, B. Singh, and X. Q. Yan, 2013: Trends in land-atmosphere interactions from CMIP5 simulations. *Journal of Hydrometeorology*, **14**, 829–849, https://doi.org/10.1175/JHM-D-12-0107.1.

Dong, J. R., W. Ni-Meister, and P. R. Houser, 2007: Impacts of vegetation and cold season processes on soil moisture and climate relationships over Eurasia. *J. Geophys. Res.*, **12**, D09106, https://doi.org/10.1029/2006JD007774.

Erdenebat, E., and T. Sato, 2018: Role of soil moisture-atmosphere feedback during high temperature events in 2002 over Northeast Eurasia. *Progress in Earth and Planetary Science*, **5**, https://doi.org/10.1186/s40645-018-0195-4.

Eyring, V., S. Bony, G. A. Meehl, C. A. Senior, B. Stevens, R. J. Stouffer, and K E. Taylor, 2016: Overview of the Coupled Model Intercomparison Project Phase 6(CMIP6) experimental design and organization. *Geoscientific Model Development*, **9**, 1937–1958, https://doi.org/10.5194/gmd-9-1937-2016.

Gu, X. H., Q. Zhang, J. F. Li, V. P. Singh, J. Y. Liu, P. Sun, C. Y. He, and J. J. Wu, 2019: Intensification and expansion of soil moisture drying in warm season over Eurasia under global warming. *J. Geophys. Res.*, **124**, 3765–3782, https://doi.org/10.1029/2018jd029776.

Guo, W. D., Z. G. Ma, and Y. H. Yao, 2003: Regional characteristics of soil moisture evolution in northern China over recent 50 years. *Acta Geographica Sinica*, **58**, 83–90, https://doi.org/10.3321/j.issn:0375-5444.2003.z1.010. (in Chinese with English abstract)

Guo, Z. C., and P. A. Dirmeyer, 2006: Evaluation of the Second

Global Soil Wetness Project soil moisture simulations: 1. Intermodel comparison. *J. Geophys. Res.*, **111**, D22S02, https://doi.org/10.1029/2006JD007233.

Hsu, P. C., T. Li, H. Murakami, and A. Kitoh, 2013: Future change of the global monsoon revealed from 19 CMIP5 models. *J. Geophys. Res.*, **118**, 1247–1260, https://doi.org/10.1002/jgrd.50145.

Huffman, G. J., and Coauthors, 1997: The Global Precipitation Climatology Project (GPCP) combined precipitation dataset. *Bull. Amer. Meteor. Soc.*, **78**, 5–20, https://doi.org/10.1175/1520-0477(1997)078<0005:TGPCPG>2.0.CO;2.

Koster, R. D., and M. J. Suarez, 2001: Soil moisture memory in climate models. *J. Hydrol.*, **2**(6), 558–570, https://doi.org/10.1175/1525-7541(2001)002<0558:SMMICM>2.0.CO;2.

Koster, R. D., M. J. Suarez, R. W. Higgins, and H. M. Van den Dool, 2003: Observational evidence that soil moisture variations affect precipitation. *Geophys. Res. Lett.*, **30**(5), 1241, https://doi.org/10.1029/2002GL016571.

Koster, R. D., and Coauthors, 2004: Regions of strong coupling between soil moisture and precipitation. *Science*, **305**, 1138–1140, https://doi.org/10.1126/science.1100217.

Koster, R. D., Z. C. Guo, R. Q. Yang, P. A. Dirmeyer, K. Mitchell, and M. J. Puma, 2009: On the nature of soil moisture in land surface models. *J. Climate*, **22**, 4322–4335, https://doi.org/10.1175/2009JCLI2832.1.

Legates, D. R., and G. J. McCabe Jr, 1999: Evaluating the use of "goodness-of-fit" measures in hydrologic and hydroclimatic model validation. *Water Resour. Res.*, **35**, 233–241, https://doi.org/10.1029/1998WR900018.

Li, Q., and S. F. Sun, 2008: Development of the universal and simplified soil model coupling heat and water transport. *Science in China Series D: Earth Sciences*, **51**, 88–102, https://doi.org/10.1007/s11430-007-0153-2.

Li, W. P., Y. W. Zhang, X. L. Shi, W. Y. Zhou, A. N. Huang, M. Q. Mu, B. Qiu, and J. J. Ji, 2019: Development of land surface model BCC_AVIM2.0 and its preliminary performance in LS3MIP/CMIP6. *Journal of Meteorological Research*, **33**(5), 851–869, https://doi.org/10.1007/s13351-019-9016-y.

Ma, Z. G., H. L. Wei, and C. B. Fu, 2000: Relationship between regional soil moisture variation and climatic variability over east China. *Acta Meteorologica Sinica*, **58**(3), 278–287, https://doi.org/10.3321/j.issn:0577-6619.2000.03.003. (in Chinese with English abstract)

Nijssen, B., R. Schnur, and D. P. Lettenmaier, 2001: Global retrospective estimation of soil moisture using the variable infiltration capacity land surface model, 1980-93. *J. Climate*, **14**, 1790–1808, https://doi.org/10.1175/1520-0442(2001)014<1790:GREOSM>2.0.CO;2.

Oglesby, R. J., and D. J. Erickson III, 1989: Soil moisture and the persistence of North American drought. *J. Climate*, **2**, 1362–1380, https://doi.org/10.1175/1520-0442(1989)002<1362:SMATPO>2.0.CO;2.

Oleson, K. W., and Coauthors, 2004: Technical description of the community land model (CLM). NCAR/TN-461+STR, 173 pp, http://dx.doi.org/10.5065/D6N877R0.

Ramillien, G., A. Cazenave, P. C. D. Milly, and A. Robock, 2003: Comparisons of soil moisture data from in situ measurements and global hydrological model outputs. Geophysical Research Abstracts, 5, 08747.

Renzullo, L. J., and Coauthors, 2014: Continental satellite soil moisture data assimilation improves root-zone moisture analysis for water resources assessment. *J. Hydrol.*, **519**, 2747–2762, https://doi.org/10.1016/j.jhydrol.2014.08.008.

Rodell, M., and Coauthors, 2004: The global land data assimilation system. *Bull. Amer. Meteor. Soc.*, **85**(3), 381–394, https://doi.org/10.1175/BAMS-85-3-381.

Ruosteenoja, K., T. Markkanen, A. Venäläinen, P. Räisänen, and H. Peltola, 2018: Seasonal soil moisture and drought occurrence in Europe in CMIP5 projections for the 21st century. *Climate Dyn.*, **50**, 1177–1192, https://doi.org/10.1007/s00382-017-3671-4.

Seneviratne, S. I., T. Corti, E. L. Davin, M. Hirschi, E. B. Jaeger, I. Lehner, B. Orlowsky, and A. J. Teuling, 2010: Investigating soil moisture-climate interactions in a changing climate: A review. *Earth-Science Reviews*, **99**, 125–161, https://doi.org/10.1016/j.earscirev.2010.02.004.

Shinoda, M., 2001: Climate memory of snow mass as soil moisture over central Eurasia. *J. Geophys. Res.*, **106**(D24), 33 393–33 403, https://doi.org/10.1029/2001jd000525.

Srinivasan, G., A. Robock, J. K. Entin, L. F. Luo, K. Y. Vinnikov, and P. Viterbo, 2000: Soil moisture simulations in revised AMIP models. *J. Geophys. Res.*, **105**, 26 635–26 644, https://doi.org/10.1029/2000JD900443.

Tawfik, A. B., and A. L. Steiner, 2011: The role of soil ice in land-atmosphere coupling over the United States: A soil moisture-precipitation winter feedback mechanism. *J. Geophys. Res.*, **116**, D02113, https://doi.org/10.1029/2010JD014333.

Taylor, K. E., 2001: Summarizing multiple aspects of model performance in a single diagram. *J. Geophys. Res.*, **106**, 7183–7192, https://doi.org/10.1029/2000JD900719.

Taylor, K. E., R. J. Stouffer, and G. A. Meehl, 2012: An overview of CMIP5 and the experiment design. *Bull. Amer. Meteor. Soc.*, **93**, 485–498, https://doi.org/10.1175/BAMS-D-11-00094.1.

Wang, A. H., and X. L. Shi, 2019: A multilayer soil moisture dataset based on the gravimetric method in China and its characteristics. *Journal of Hydrometeorology*, **20**, 1721–1736, https://doi.org/10.1175/JHM-D-19-0035.1.

Wu, T. W., and Coauthors, 2013: Global carbon budgets simulated by the Beijing Climate Center Climate System Model for the last century. *J. Geophys. Res.*, **118**, 4326–4347, https://doi.org/10.1002/jgrd.50320.

Wu, T. W., and Coauthors, 2014: An overview of BCC climate system model development and application for climate change studies. *Journal of Meteorological Research*, **28**, 34–56, https://doi.org/10.1007/s13351-014-3041-7.

Wu, T. W., and Coauthors, 2019: The Beijing Climate Center Climate System Model (BCC-CSM): The main progress from CMIP5 to CMIP6. *Geoscientific Model Development*, **12**, 1573–1600, https://doi.org/10.5194/gmd-12-1573-2019.

Wu, T. W., and Coauthors, 2020: Beijing Climate Center Earth System Model version 1(BCC-ESM1): Model description and evaluation of aerosol simulations. *Geoscientific Model Development*, **13**, 977–1005, https://doi.org/10.5194/gmd-13-977-2020.

Xia, Y. L., M. B. Ek, Y. H. Wu, T. Ford, and S. M. Quiring, 2015: Comparison of NLDAS-2 simulated and NASMD observed daily soil moisture. Part I: Comparison and analysis. *Journal of Hydrometeorology*, **16**, 1962–1980, https://doi.org/10.1175/JHM-D-14-0096.1.

Xin X. G., T. W. Wu, and J. Zhang, 2012: Introduction of CMIP5 experiments carried out by BCC Climate System Model. *Progressus Inquisitiones de Mutatione Climatis*, **8**(5), 378–382,

https://doi.org/10.3969/j.issn.1673-1719.2012.05.010. (in Chinese with English abstract)

Xin, X. G., and Coauthors, 2019: Introduction of BCC models and its participation in CMIP6. *Climate Change Research*, **15**(5), 533–539, https://doi.org/10.12006/j.issn.1673-1719.2019.039. (in Chinese with English abstract)

Yeh, T. C., R. T. Wetherald, and S. Manabe, 1984: The effect of soil moisture on the short-term climate and hydrology change–A numerical experiment. *Mon. Wea. Rev.*, **112**, 474–490, https://doi.org/10.1175/1520-0493(1984)112<0474:TEOSMO>2.0.CO;2.

Yuan, S. H., and S. M. Quiring, 2017: Evaluation of soil moisture in CMIP5 simulations over the contiguous United States using in situ and satellite observations. *Hydrology and Earth System Sciences*, **21**, 2203–2218, https://doi.org/10.5194/hess-21-2203-2017.

Zhang, J. Y., W. C. Wang, and J. F. Wei, 2008: Assessing land-atmosphere coupling using soil moisture from the Global Land Data Assimilation System and observational precipitation. *J. Geophys. Res.*, **113**, D17119, https://doi.org/10.1029/2008JD009807.

Zhang, R. H., R. N. Zhang, and Z. Y. Zuo, 2016a: An overview of wintertime snow cover characteristics over China and the impact of Eurasian snow cover on Chinese climate. *Journal of Applied Meteorological Science*, **27**(5), 513–526, https://doi.org/10.11898/1001-7313.20160501. (in Chinese with English abstract)

Zhang, S. W., Y. Liu, B. J. Cao, and S. Y. Li, 2016b: Soil moisture-precipitation coupling and trends in China, based on GLDAS and CMIP5 products. *Climatic and Environmental Research*, **21**(2), 188–196, https://doi.org/10.3878/j.issn.1006-9585.2015.15112. (in Chinese with English abstract)

Zuo, Z. Y., and R. H. Zhang, 2007: The spring soil moisture and the summer rainfall in eastern China. *Chinese Science Bulletin*, **52**(23), 3310–3312, https://doi.org/10.1007/s11434-007-0442-3.